Journal Pre-proof

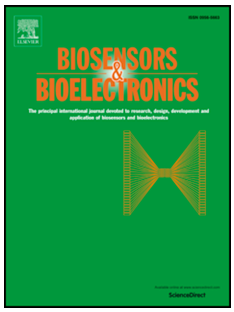

Fullerenol as a photoelectrochemical nanoprobe for discrimination and ultrasensitive detection of amplification-free single-stranded DNA

Hai-Hua Wang, Meng-Jie Li, Yu-Peng Tu, Hai-Jun Wang, Ya-Qin Chai, Zhao-Hui Li, Ruo Yuan

PII: S0956-5663(20)30789-2

DOI: https://doi.org/10.1016/j.bios.2020.112802

Reference: BIOS 112802

To appear in: *Biosensors and Bioelectronics*

Received Date: 17 July 2020

Revised Date: 27 October 2020

Accepted Date: 3 November 2020

Please cite this article as: Wang, H.-H., Li, M.-J., Tu, Y.-P., Wang, H.-J., Chai, Y.-Q., Li, Z.-H., Yuan, R., Fullerenol as a photoelectrochemical nanoprobe for discrimination and ultrasensitive detection of amplification-free single-stranded DNA, *Biosensors and Bioelectronics* (2020), doi: https://doi.org/10.1016/j.bios.2020.112802.

CRediT Author Statement

Hai-Hua Wang: Conceptualization; Methodology; Investigation; Data Collection, Curation and Analysis; Discussion; Validation; Writing-Original Draft Preparation; Writing-Reviewing and Editing; Formal Analysis

Meng-Jie Li: Discussion; Writing-Reviewing and Editing; Formal Analysis

Yu-Peng Tu: Investigation; Data Collection; Discussion

Hai-Jun Wang: Discussion

Ya-Qin Chai: Supervision; Project Administration; Funding Acquisition; Writing-Reviewing and Editing; Discussion

Zhao-Hui Li: Supervision; Project Administration; Discussion

Ruo Yuan: Supervision; Principle Investigator; Resources; Project Administration; Funding Acquisition; Data Curation and Analysis; Discussion; Writing-Reviewing and Editing

Fullerenol as a Photoelectrochemical Nanoprobe for Discrimination and Ultrasensitive Detection of Amplification-Free Single-Stranded DNA

Hai-Hua Wang,[†] Meng-Jie Li,[†] Yu-Peng Tu,[†] Hai-Jun Wang,[†] Ya-Qin Chai,[†] Zhao-Hui Li,[*,‡] and Ruo Yuan[*,†]

† Key Laboratory of Luminescence Analysis and Molecular Sensing (Southwest University), Ministry of Education, College of Chemistry and Chemical Engineering, Southwest University, Chongqing 400715, P.R. China

Email address: yuanruo@swu.edu.cn (R. Yuan)

Tel.: +86-23-68252277; Fax.: +86-23-68253172.

‡ Henan Joint International Research Laboratory of Green Construction of Functional Molecules and Their Bioanalytical Applications, College of Chemistry, Zhengzhou University, Zhengzhou 450001, P.R. China

Email address: zhaohui.li@zzu.edu.cn (Z. H. Li)

Abstract

Traditional approaches for nucleic acids detection require prior amplification of target genes, while nanomaterials-aided DNA biosensors are very magnificent but still suffer from the nanomaterial acquirement and limited sensitivity (above picomolar level). Herein, fullerenol $C_{60}(OH)_{25}$, a representative fullerene derivative, was employed as a photoelectrochemical (PEC) nanoprobe to achieve discrimination and ultrasensitive detection of amplification-free single-stranded DNA (ssDNA) down to sub-femtomolar level. The bonded hydroxyl groups with intense density endowed fullerenol to directly recognize and capture ssDNA-AuNPs *via* the hydrogen bonding interactions (H-bonds), leading to a sharply

decreased photocurrent with quenching efficiency up to 85%, which could be attributed to the photo-generated electrons on the conduction band of fullerenol (-4.66 eV) preferentially migrating to the Fermi level of AuNPs (-5.1 eV) rather than the electrode. In the presence of target gene (mutant human p53 gene fragment), the H-bonds between fullerenol and ssDNA were competitively depleted during the base pairing process of complete hybridization between ssDNA and target, making double-stranded DNA-AuNPs (dsDNA-AuNPs) depart so that the photocurrent powerfully recovered. On basis of the photocurrent variation before and after target introduction, this proposed simple, rapid and ultrasensitive PEC biosensor for amplification-free target gene detection illustrated a wide liner ranged from 1 fM to 100 pM and a detection limit of 0.338 fM. This work presented an ingenious strategy for the discrimination and ultrasensitive detection of nucleic acids, and the well-designed PEC biosensor was further conducive to the impetus of clinic diagnostics.

Keywords: fullerenol; nucleic acids discrimination; amplification-free; photoelectrochemical biosensor; gold nanoparticles; electron transfer

1. Introduction

Biomolecular detection is becoming eventful in nanotechnology, biomedicine, environmental monitoring and clinic diagnostics (Tavallaie et al., 2018; Willner et al., 2007), which has motivated increasing enthusiastic in the advancement of simple, rapid and sensitive biosensors for various biomarkers analysis implicating small molecules, proteins and nucleic acids (Chen et al. 2020; Li et al., 2018; Zhang et al., 2019; Zhu et al., 2020). With respect to nucleic acids detection, various powerful methods have been raised, such as quantitative polymerase chain reaction (qPCR; the current gold-standard), isothermal amplification, and

next-generation sequencing. However, these traditional approaches require prior amplification of target genes and well-equipped laboratories, making the examination procedures fairly complicated. Very recently, clustered regularly interspaced short palindromic repeats-Cas (CRISPR-Cas) technology, holding great significance in gene editing, also shows potential for the highly selective and sensitive determination of nucleic acids (Bruch et al., 2019a; Zetsche et al., 2015). Thanks for its programmability through a single-guide RNA or a pre-CRISPR RNA, CRISPR-Cas system enables simple, easily scalable and amplification-free channel for building nucleic acids biosensing devices (Bruch et al., 2019b; Wang et al., 2020). Besides, it is worth to note that coupling nanomaterials with direct nucleic acids recognition also opens up bright opportunities for the fabrication of simple, rapid and high-performance nucleic acids biosensors (Ho et al., 2019; Mal et al., 2018).

In the past decade, highlighted by the appreciative discrimination capability towards single-stranded DNA and double-stranded DNA (ssDNA/dsDNA), various nanomaterials have been synthesized and developed for the sensitive and selective detection of ssDNA, involving transition metal dichalcogenides (TMDs) such like MoS_2 (Zhu et al., 2013), and TaS_2 (Zhang et al., 2015), metal-organic framework (MOF) (Zhao et al., 2015), covalent organic framework (COF) (Peng et al., 2017), *etc.*. Besides, carbon nanomaterials in different dimension, as exemplified by two-dimension (2D) graphene oxide (GO) (Li et al., 2013; Wang et al., 2016), and graphdiyne (GD) (Parvin et al., 2017), 1D carbon nanotubes (CNTs) (Tang et al., 2014; Yang et al., 2008), as well as 0D carbon quantum dots (CQDs) (Ouyang et al., 2012), have been employed as a class of intriguing candidates to recognize nucleic acids (Sun et al., 2016). For the discrimination principle, ssDNA could be directly absorbed on the nanomaterials surface with certain strong interactions, while dsDNA would be released and

away from the nanomaterials due to the vanished interactions after ssDNA was hybridized. Thanks to this merit, the subsequently established biosensors for ssDNA detection exhibited simple operation and rapid response with the assist of a signal indicator. In despite of these distinct achievements, however, it is disappointed that the preparation processes of some nanomaterials mentioned are strict with the prerequisite requirement of sophisticated instruments. More importantly, these biosensing platforms still suffer from the limited detection sensitivity exclusively at above-picomolar level, which inevitably hinder their wide implements in the practical examinations, considering the concentration of target nucleic acids might at femtomolar range (Hwang et al., 2020). The reason behind these unsatisfied detection limits could be mainly attributed to the inherent shortages of traditionally optical detection method (fluorescence), which entails the same form of excited source and detectable signal, causing severe cross-disturbance and high background signals. Thereby, the achievement of more accessible and sensitive detection for nucleic acids is imperatively expected.

Photoelectrochemical (PEC) bioanalysis is ascendant and attractive because of the totally separated and different energy forms between the excited source (light) and the reported signal (current), leading to extremely low background signals of the constructed biosensor, which gives insights to the detection limit reduction and sensitivity improvements (Wang et al., 2018; Wen et al., 2018; Zhao et al., 2014). Fullerenol $C_{60}(OH)_{25}$ is a typical hydroxylation derivative of 0D fullerene C_{60} belonging to the carbon nanomaterials. With unique nanostructure and nearly cognate physicochemical features as fullerene, fullerenol owns more remarkable performance on high biocompatibility, surface energetic active sites and superb electron accommodation (Niu et al., 2011). In this work, fullerenol $C_{60}(OH)_{25}$ was employed

as a PEC nanoprobe to selectively discriminate ssDNA/dsDNA, with the help of highly quenching efficiency of Au nanoparticles (AuNPs) against fullerenol to construct a simple, rapid and ultrasensitive PEC biosensor for amplification-free ssDNA detection. **Scheme 1** showed the detection principle. Two ssDNAs including mutant human p53 gene fragment as the target (T) and its complementary probe (P1) with the terminal labeled by AuNPs (defined as P1-AuNPs) were used to construct the PEC biosensor. As seen, the prepared fullerenol exhibited an initial photocurrent response. When P1-AuNPs was decorated on the modified electrode, fullerenol directly captured P1-AuNPs through the intense hydrogen bonding interactions (H-bonds) formed between rich hydroxyl groups (-OHs) of fullerenol and the nucleic bases of P1, leading to a sharp decrement of photocurrent response with a PEC quenching efficiency up to 85%. In rationale, the PEC quenching mechanism behind this system was ascribed to the visible light-induced electron transfer from the conduction band of fullerenol to the Fermi level of AuNPs. In the presence of T, T was hybridized with P1 to yield T/P1-AuNPs that would depart from the modified electrode, since the H-bonds between fullerenol and P1 was competitively depleted during the complete base pairing process. This caused an effective recovery of photocurrent response, which was used to quantitatively evaluate T. The proposed PEC biosensor displayed simple, rapid and ultrasensitive for the determination of p53 gene fragment, coupling with a wide liner range from 1 fM to 100 pM and a detection limit down to 0.338 fM.

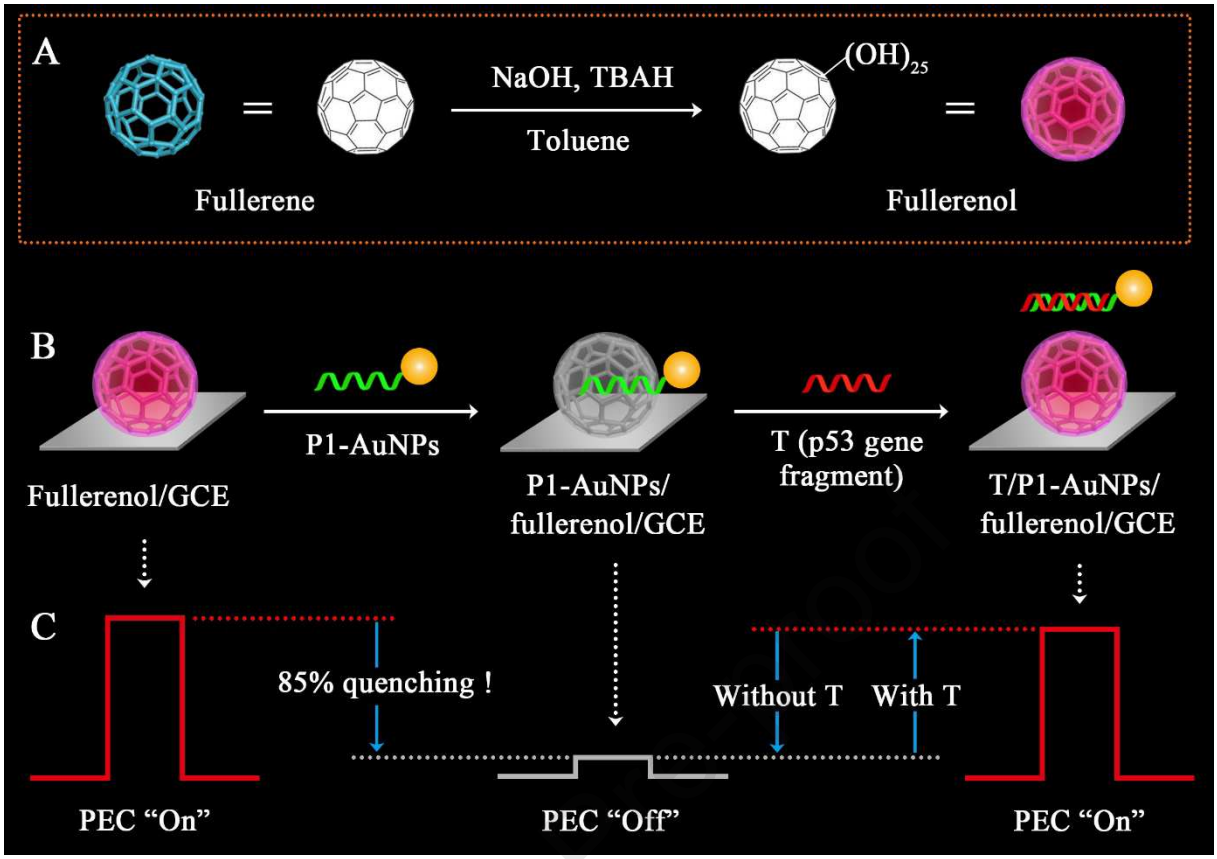

Scheme 1. Schematic representation of the synthesis route from fullerene to fullerenol (A) and the fabrication process of the fullerenol-based PEC biosensor (B), with the photocurrent responses of multi-step modified electrodes with "on-off-on" model (C).

2. Results and Discussion

2.1. Nanomaterials Characterizations

From the ultraviolet-visible (UV-vis) absorption spectrums, three characteristic absorption peaks located at 440 nm, 346 nm and 268 nm were observed for fullerene (Fig. 1A), while a novel and exclusive absorption peak at 224 nm was exhibited for fullerenol (Fig. 1B), revealing the successful functionalization of –OHs on fullerenol. According to the tangent study against the maximum absorption, 397 nm was corroborated as the initial optical absorption wavelength (denoted as λ_{onset}) of fullerenol. Dynamic light scattering (DLS)

measurements indicated an obvious increment in particle size of fullerenol with the average size of 275.9 nm (Fig. 1D) in contrast to fullerene with the average size of 129.7 nm (Fig. 1C), mainly because of the more intense aggregation tendency of fullerenol in the aqueous phase. Besides, zeta potential (ZP) in -17.6 mV of fullerene and -26.8 mV of fullerenol (Fig. 1E) demonstrated their good stability in aqueous medium, when the increment of ZP of fullerenol versus fullerene depicted the better binding affinity of fullerenol than that of fullerene. As seen from the X-ray photoelectron spectroscopy (XPS) of fullerenol (Fig. 1F), two expected peaks of the binding energies at 284.85 eV and 536 eV were found, of which the former belonged to C1s and the latter belonged to O1s, which represented the existence of oxygen and carbon atoms in fullerenol. In addition, Fourier transform infrared spectroscopy (FTIR) spectrum of fullerenol was obtained in Fig. S2, where several typical bands at the related wavenumbers were depicted, containing 3410 cm^{-1} for $\nu_{\text{-OH}}$, 1594 cm^{-1} for $\nu_{C=C}$, 1374 cm^{-1} for $\sigma_{\text{C-O-H}}$, and 1074 cm^{-1} for $\nu_{\text{C-O}}$. All these results proved the successful synthesis from fullerene to fullerenol by the one-step facile synthesis. The number of -OHs on single fullerenol was calculated as 25 according to the XPS atom% value of fullerenol, thus the molecular formula of fullerenol was presumed as $C_{60}(OH)_{25}$.

The electrochemical and PEC activities of fullerenol were further censored. According to the electrochemical impedance spectroscopy (EIS) in Fig. 1G, fullerenol elaborated a smaller semicircle diameter in contrast to fullerene, implying superior electron transmission capability and surface reaction kinetics of fullerenol due to the modification of rich -OHs. Importantly, considering the homology of carbon nanomaterials, a comparison study for the photocurrent responses of fullerenol and other typical carbon nanomaterials in different dimensions and nanostructures was executed, as shown in Fig. 1H. Under the optimized experimental

conditions (details in Fig. S3), photocurrent intensity of 0.63 μA (curve e) for 0D fullerenol was obtained, which was distinctly stronger than that of other chosen carbon nanomaterials, involving 0.23 μA for 2D GO (curve a), 0.24 μA for 1D CNT (curve b), 0.08 μA for 0D CQD (curve c) and 0.50 μA for 0D fullerene (curve d). Reasonably, the improved PEC performance of fullerenol could be ascribed to its superior photoelectric activity of increased surface energetic active sites and superb electron transmission. For the characterization of AuNPs, scanning electron microscopy (SEM) image and UV-vis absorption spectrum were conducted. As shown in Fig. S4, AuNPs possessed uniform global morphology in the size of 16 nm and a surface plasmonic absorption location at 523 nm.

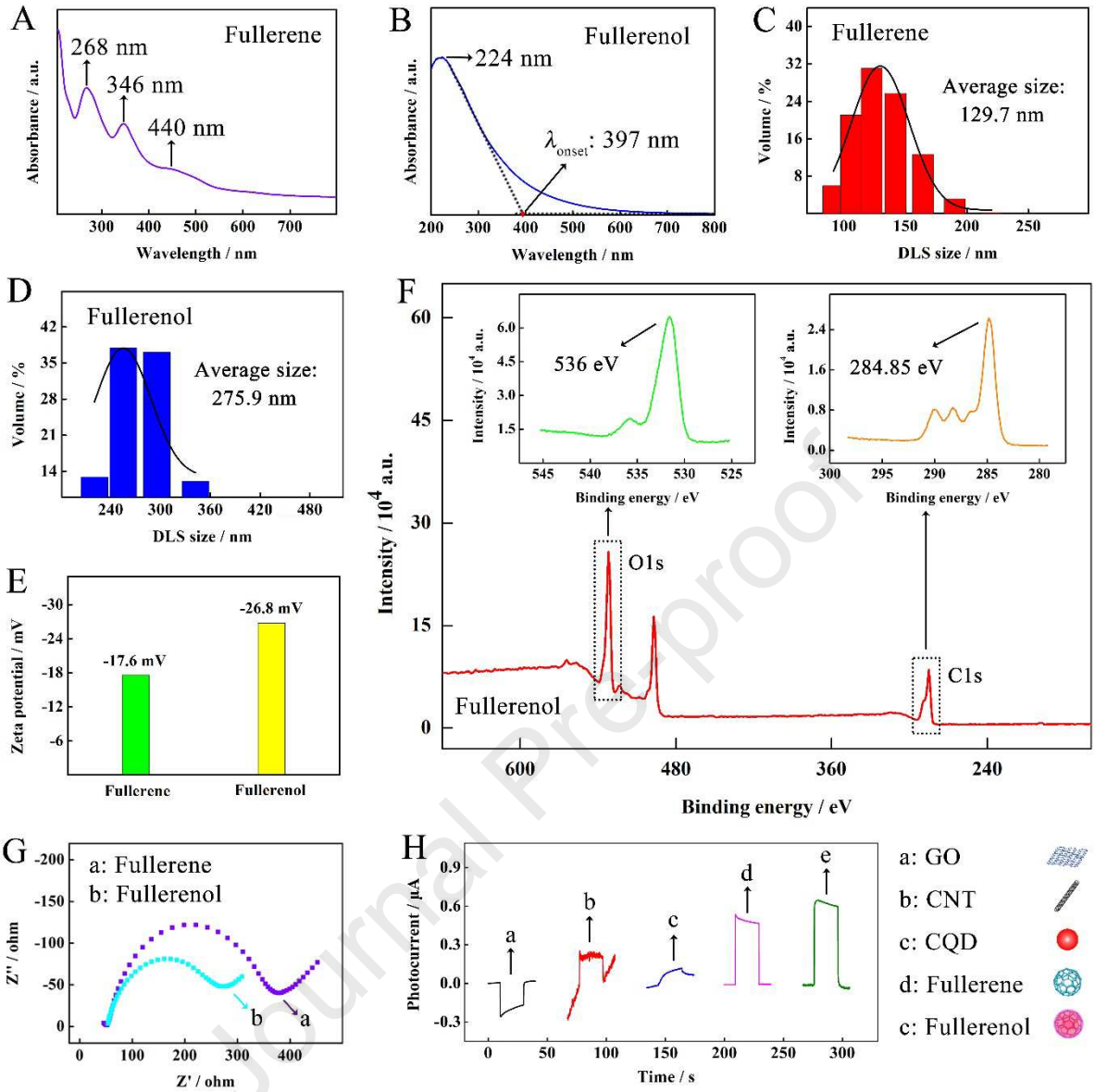

Fig. 1. UV-vis absorption spectrums of fullerene (A) and fullerenol (B). DLS size distributions of fullerene (C) and fullerenol (D). ZPs (E) of fullerene (left) and fullerenol (right). XPS spectrum of fullerenol (F), with the high-resolution XPS spectrums of O1s and C1s in inset. EIS curves (G) of fullerene (a) and fullerenol (b). Photocurrent responses of various carbon nanomaterials (H): 2D GO (a), 1D CNT (b), 0D CQD (c), 0D fullerene (d) and 0D fullerenol (e).

2.2. Methodology and Characterization of the PEC Biosensor

The feasibility of the complete hybridization between T and P1 (the probe sequences were seen in Table S1) was confirmed by native polyacrylamide gel electrophoresis (PAGE) method, and the resultant image was placed in Fig. 2A. T (lane 1) and P1 (lane 2) presented the same migration distance for the same bases number of T and P1, while the mixture of T and P1 (lane 3) exhibited much slower movement, which indicated the hybridization between T and P1. The PEC biosensing behaviors were evidenced by the changed photocurrent responses of the multi-step modified electrodes, as illustrated in Fig. 2B. At the beginning, the glass carbon electrode (GCE) modified with fullerenol (fullerenol/GCE) exhibited a promising photocurrent response of 0.63 μA (curve a). After the subsequent immobilization of P1-AuNPs (P1-AuNPs/fullerenol/GCE), P1-AuNPs was directly absorbed on fullerenol through the energetic H-bonds formed between fullerenol and P1, and the photocurrent response turned into only 0.095 μA (curve b) with the calculated PEC quenching efficiency up to 85%. Such a sharp photocurrent attenuation suggested the great PEC quenching effect of AuNPs against fullerenol based on the visible light-induced electron transfer from fullerenol to AuNPs. Ultimately, a reinstated photocurrent response of 0.59 μA (curve c) was found when the modified electrode was further incubated with T (T/P1-AuNPs/fullerenol/GCE). Upon the complete hybridization of T and P1 for T/P1 duplex, the reinstated photocurrent could be caused by the departure of T/P1-AuNPs from fullerenol. Consequently, on account of the photocurrent variations before and after incubating T at a range of different concentrations, a simple, rapid and ultrasensitive PEC biosensor was proposed for T determination.

Cyclic voltammetry (CV) process was measured to characterize the multi-step construction of the PEC biosensor (Fig. 2C). Initially, the pretreated GCE exhibited a pair of redox peak (curve a) with a strong intensity. As for the fullerenol/GCE, the peak current (curve b) was apparently declined owing to the hinder effect of fullerenol against the electron transmission. Subsequently, when P1-AuNPs was immobilized (P1-AuNPs/fullerenol/GCE), an evident enhancement of peak current (curve c) was gotten in view of the exceptional conductivity of AuNPs. Lastly, after T was introduced (T/P1-AuNPs/fullerenol/GCE), the peak current (curve d) was observed to recovery, whose current intensity was proximate to that of fullerenol/GCE, attributing to the release of T/P1-AuNPs complex from the modified electrode surface. These results suggested the successful fabrication of the PEC biosensor.

2.3. ssDNA/dsDNA Discrimination

SEM, DLS size, and ZP were applied to verify and elaborate the discriminating events of fullerenol towards ssDNA and dsDNA. From the SEM images, the prepared fullerenol exhibited spherical shape with good dispensability, and its diameter was approximately across 30 nm to 60 nm (Fig. 2D). For the mixture of fullerenol and P1, the diameter sharply increased to about 100-200 nm (Fig. 2E), which was much larger than that of fullerenol alone. This obvious enlargement in size distribution conclusively implied that the strong H-bonds led to the vivid interactions between fullerenol and P1, i.e., the assembly of P1-fullerenol. Interesting to note, after the further introduction of T, the size distribution for the mixture of fullerenol, P1 and T (Fig. 2F) was close to that of fullerenol alone, which demonstrated no obvious association between T/P1 duplex and fullerenol. These results provided a powerful verification for the absorption preference of fullerenol towards ssDNA than dsDNA. Besides,

DLS size and ZP were also conducted to study the ability of fullerenol to discriminate the nucleic acids in different configurations. Specifically, the mixture of fullerenol and P1 showed the average size of 480.7 nm (Fig. 2G) with the ZP of -34.6 mV (Fig. 2I). Compared to the average size of 275.9 nm (Fig. 1D) and the ZP of -26.8 mV (Fig. 1E) of fullerenol, the increment on the average size of the mixture of fullerenol and P1 again indicated the assembly of P1-fullerenol in the aqueous medium, and the enhancement about the ZP suggested the increment of negatively charge density of fullerenol surface, furthermore presenting the surface coverage of fullerenol by P1. For the mixture of fullerenol, P1 and T, the average size was 309.9 nm (Fig. 2H) and the ZP was -28.4 mV (Fig. 2I), which manifested the detached state between fullerenol and the hybridized T/P1 duplex. All the consequences of DLS sizes and ZPs in agreement with the SEM results highlighted the dramatic screening capability of fullerenol towards the nucleic acids in different configurations, demonstratively with ssDNA capture but dsDNA release.

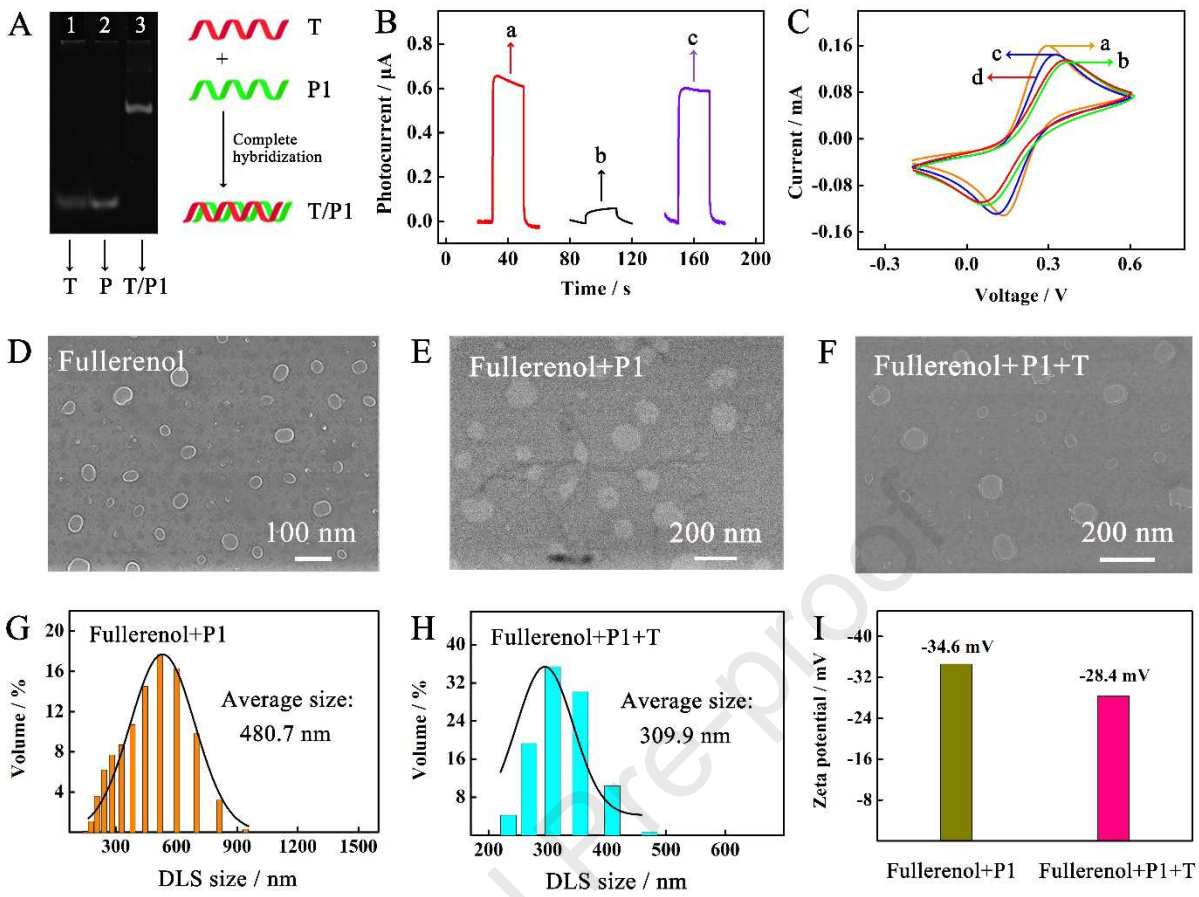

Fig. 2. Native PAGE image of lane 1 for T, lane 2 for P1, and lane 3 for T/P1 duplex (A). Photocurrent responses of the PEC biosensor (B): fullerenol/GCE (a), P1-AuNPs/fullerenol/GCE (b) and T/P1-AuNPs/fullerenol/GCE (c). CV responses of the PEC biosensor (C): the pretreated GCE (a), fullerenol/GCE (b), P1-AuNPs/fullerenol/GCE (c) and T/P1-AuNPs/fullerenol/GCE (d). SEM images of fullerenol (D), fullerenol+P1 (E) and fullerenol+P1+T (F). DLS size distributions of fullerenol+P1 (G) and fullerenol+P1+T (H). ZPs (I) of fullerenol+P1 (left) and fullerenol+P1+T (right).

2.4. Interactions between Fullerenol and ssDNA/dsDNA

The existed interactions between fullerenol and ssDNA/dsDNA were undertaken by the UV absorption spectrums, as illustrated in Fig. S5. P1 owned an evidence absorption peak at 260 nm (Fig. S5A), which was consistent with the characteristic absorption of

oligonucleotides. While P1 and T was mixed, the absorption peak changed to 257 nm (Fig. S5B), where the 3 nm blue-shift was inferentially induced by the formed H-bonds during the nucleic bases pairing process between P1 and T. Notably, compared to the absorption peak of pure P1, the mixture of fullerenol and P1 showed 6 nm blue-shift with the absorption peak at 254 nm (Fig. S5C). This fact elaborated the direct capture of P1 by fullerenol through the dense H-bonds between rich -OHs of fullerenol and the nucleic bases of P1 (-OH···X; X = N, O…). After the further addition of T, the nucleic bases pairing between P1 and T totally competed the H-bonds between fullerenol and P1, thereby T/P1 duplex was separated from fullerenol, making the absorption peak of 256 nm in Fig. S5D approach 257 nm in Fig. S5B as the characteristic absorption of T/P1. These results confirmed that fullerenol captured P1 through hydrogen-bonding interactions but released T/P1, thus achieving the selective discrimination of ssDNA/dsDNA. Though fullerene was also announced to capture nucleic acids through π-π stacking interactions, however, the efficiency of subsequent hybridization was not very high, which would impede the achievement of ultrasensitive T detection (Kaisti, 2017). Furthermore, the UV absorption peak of the mixture of fullerene and P1 was located at 263 nm as seen in Fig. S6, specifying merely 3 nm red-shift versus P1 alone, which proved more vigorous immobilization for the ssDNA on fullerenol through hydrogen-bonding interactions (6 nm blue-shift) than on fullerene through π-π stacking interactions. This merit was reasonably attributed to the integration of the ultrahigh surface density of -OHs on single fullerenol and the flexible single nucleic acid strand.

2.5. Visible Light-Induced Electron Transfer for Photocurrent Responses

In view of the changed photocurrent generated by the multi-step modified electrodes,

mainly involving fullerenol/GCE and P1-AuNPs/fullerenol/GCE, feasible mechanisms of visible light-induced electron transfer were raised for the photocurrent responses. In advance, the energy band gap (E_g) and the energy levels of conduction band (E_{CB}), valence band (E_{VB}), and Fermi level (E_F) of fullerenol were investigated (Fig. S7). The energy band diagram for fullerene (Wang et al., 2019), fullerenol and AuNPs (Clavero, 2014), was summarized in Fig. 3A. Notably, there were obvious divergence of the energy structure between fullerene and fullerenol, and the E_{CB} of fullerenol (-4.66 eV) was interestingly much lower than that of fullerene (-3.7 eV), which could be attributed to the surface functionalization of fullerenol with rich –OHs. Fig. 3B proposed the mechanism of photocurrent response for fullerenol/GCE. In a typical procedure, the photo-generated electrons (e^-) in the CB and the photo-generated holes (h^+) in the VB of fullerenol were produced under 460 nm-light illumination. Subsequently, the e^- migrated to the GCE (route I, Fig. 3B) and the h^+ could be digested by AA. Hence, the electron transfer route was completed, causing the photocurrent response. As for the establishment of P1-AuNPs/fullerenol/GCE, AuNPs was proximate to fullerenol, making a PEC quenching system, whose possible electron transfer mechanism was decorated in Fig. 3C. On this occasion, the e^- in the fullerenol CB would preferentially move to the Fermi level (E_F) of AuNPs (route □, Fig. 3C) instead of the GCE (route □, Fig. 3C), and the e^- in AuNPs E_F was subsequently trapped by the dissolved oxygen (O_2) in detection electrolyte. The dissolved O_2 was then reduced, and the superoxide free radical ($O_2^{\bullet -}$) emerged (Fig. S8). Consequently, only a bit number of e^- could reach to the GCE, yielding a sharply decreased photocurrent. Furthermore, the transient photocurrent responses and *I-T* (where *I* was the photocurrent and *T* was the time) curves for fullerenol/GCE and P1-AuNPs/fullerenol/GCE were implemented. As shown in Fig. 3D and 3E, the gained

photocurrent responses had exceptional retention even as the illuminated time surpass 300 s, indicating the promising stability and durability of the multi-step fabricated PEC biosensor. Some control experiments were further conducted about the photocurrent responses using P1-AuNPs to modify different CNM, and the results showed vivid PEC quenching effect of AuNPs towards fullerenol. Additionally, the photocurrent variations were quite in divergence, which may originated from the different immobilization intensity and PEC interacting effect (Fig. S8).

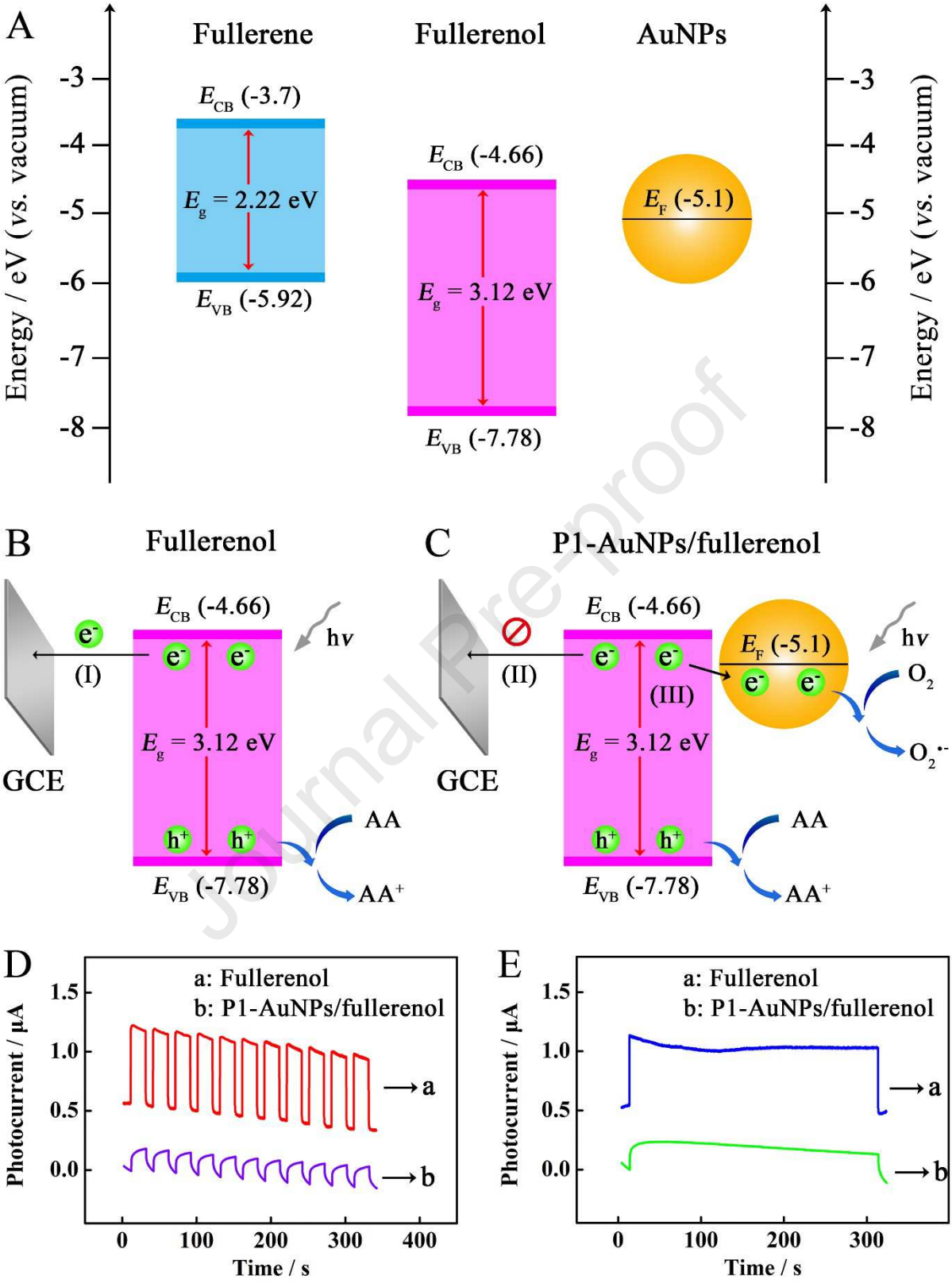

Fig. 3. Energy band diagram for fullerene, fullerenol and AuNPs (A). Feasible mechanism of visible light-induced electron transfer for fullerenol/GCE (B) and P1-AuNPs/fullerenol/GCE (C). Transient photocurrent responses (D) and *I-T* curves (E) of fullerenol (a) and

P1-AuNPs/fullerenol (b). The transient photocurrent responses were conducted under the periodic "off-on-off" switch mode of 10-20-10 s for 11 cycles. The *I-T* curves were implemented under the "off-on-off" switch mode of 10-300-10 s.

2.6. Analysis Performance of the PEC Biosensor

In order to evaluate the analysis performance of the constructed PEC biosensor, series concentrations of T (p53 gene fragment) was incubated onto the P1-AuNPs/fullerenol/GCE, and the photocurrent responses were examined (Fig. 4). As exhibited in Fig. 4A, the photocurrent intensity was gradually improved in pace with the increased concentration of T from 1 fM to 100 pM. Fig. 4B described that the linear relationship was fitted as $I = 0.6690 + 0.08082 \lg c$ (where I and c were the photocurrent intensity and the concentration of T, respectively) with the correlation coefficient (R^2) of 0.9948. Under a definition of limit of detection (LOD) = $\text{mean}_{\text{blank}} + 1.645(\text{SD}_{\text{blank}}) + 1.645(\text{SD}_{\text{low concentration sample}})$ (Armbruster and Pry, 2008), the LOD down to 0.338 fM could be calculated for T detection. A detailed comparative survey on the analysis performance for our fabricated PEC biosensor with other published works for nucleic acids determination was then conducted. In contrast to not only the works based on different substance-aided ssDNA/dsDNA discrimination (Table 1), but also the works using different signal reporters (Table S2), our PEC biosensor owned much lower LOD, signifying the superior sensitivity of our PEC biosensor. There were three major reasons for the ultrasensitivity achieved, the inherent merit of PEC assay, the significant ssDNA/dsDNA discrimination capability of fullerenol, and the powerful PEC quenching efficiency of AuNPs against fullerenol. Besides, T (10 pM) and its interferences including single-based mismatch probe 1 (P2, 1 nM), single-based mismatch probe 1 (P3, 1 nM),

double-based mismatch probe (P4, 1 nM) as well as the mixture (the mixture of P2, P3, P4 and T) (the probe sequences were seen in Table S1) were employed to verify the selectivity of the PEC biosensor. From Fig. 4C and 4D, the introduction of T and the mixture caused high photocurrent responses, while other samples resulted in slight photocurrent responses, implying that only T instead of the interferences enabled the signal quencher release, which suggested the excellent selectivity of the PEC biosensor. The duplicated photocurrent response of the PEC biosensor incubated with 100 pM T (Fig. S10) proved the satisfying long-term stability. As tabulated in Table S3, the PEC biosensor was employed to validate the content of added T in human serum samples as a real application through the standard recovery test, where ssDNA modification could protect AuNPs from aggregating. Under T addition at different concentration levels in the human serum samples, the recovery ranged from 97.29% to 108.67% and the RSDs no more than 2.84% revealed promising reliability of the PEC biosensor in the quantitative evaluation of nucleic acids, which thus could be expanded to the practical implements. The promising analysis performance of the constructed PEC biosensor suggested the value of our strategy for the discrimination and ultrasensitive detection of nucleic acids.

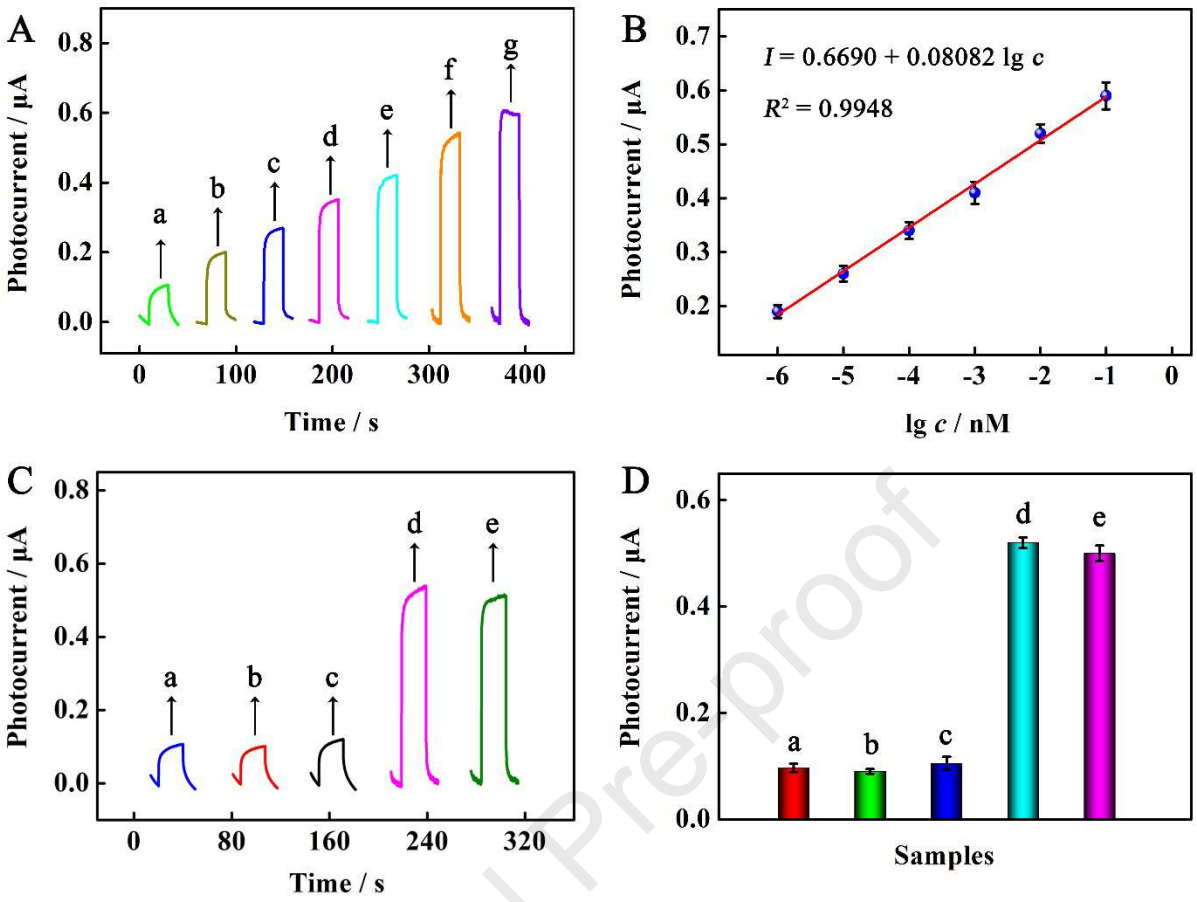

Fig. 4 Photocurrent responses of the PEC biosensor at different concentrations of T (A): zero (a), 1 fM (b), 10 fM (c), 100 fM (d), 1 pM (e), 10 pM (f) and 100 pM (g). The linear relationship between photocurrent intensity and concentration logarithm of T (B). Photocurrent responses (C) and the selectivity (D) of the PEC biosensor incubated with different samples: P2 (1 nM) (a), P3 (1 nM) (b), P4 (1 nM) (c), T (10 pM) (d) and the mixture (e).

Table 1. Comparative study of the proposed PEC biosensor with other works based on different substance-aided ssDNA/dsDNA discrimination for oligonucleotide detection.

Substance	Type	Model	LOD	Ref.
MoS_2	2D	DNA	500 pM	Zhu et al., 2013
TaS_2	2D	DNA	50 pM	Zhang et al., 2015
Cu-TCPP MOF	2D	DNA	20 pM	Zhao et al., 2015
TPA-COF	2D	DNA	20 pM	Peng et al., 2017
GO	2D	DNA	0.17 nM	Wang et al., 2015
GD	2D	DNA	25 pM	Parvin et al., 2017
GD oxide	2D	DNA	84 pM	Wang et al., 2016
GD oxide	2D	DNA	17 pM	Wang et al., 2016
citric acid CQD	0D	DNA	45.6 nM	Lo et al., 2016
malic acid CQD	0D	DNA	17.4 nM	Lo et al., 2016
Fullerenol	0D	DNA	**0.338 fM**	***This work***

Note that there were two target sequences in Ref. Wang et al., 2016 and Ref. Lo et al., 2016, respectively.

3. Conclusion

In couclusion, this work comprehensively investigated the bioanalysis application of fullerenol (rich hydroxylated fullerene) as a PEC nanoprobe to achieve discrimination and ultrasensitive detection of amplification-free ssDNA. On the one hand, fullerenol was highlighted by the discrimination ability towards nucleic acids under the modulation of H-bonding interactions; thus ssDNA recognition but dsDNA departure was realized, making the constructed PEC biosensor much simple and rapid with low background. On the other hand, the photocurrent response was intensely inhibited using AuNPs as the signal quencher in view of visible light-induced electron transfer, which was conspicuously beneficial to the improvement of detection sensitivity. Besides, the high selectivity and specificity were

achieved by the pre-designed comlementary sequence that could be directly absorbed on fullerenol and only binded to the tagert gene. Ultimately, the proposed PEC biosensor for the determination of p53 gene fragment owned a wide liner range from 1 fM to 100 pM and a LOD down to 0.338 fM, and acquired dependable results in the preliminary application with assistance of human serum samples. While future work will be demanded, for example, to measure the interaction force between fullerenol and ssDNA or to alter target sequence, this ingenious strategy represented a critical step toward the discrimination and ultrasensitive detection of nucleic acids, which could broaden biomolecule recognition and enrich biosensing technology, opening up attractive advancement in the clinic diagnostic.

Acknowledge

This work was financially supported by the National Natural Science Foundation of China (21974108, 21775124 and 21675129) and the Fundamental Research Funds for the Central Universities (XDJK2020TY002), China.

Declaration of interests

The authors declare no conflict of interests.

References

Armbruster, D.A.; Pry, T., 2008. Clin. Biochem. Rev. 29, S49−S52.

Bruch, R., Baaske, J., Chatelle, C., Meirich, M., Madlener, S., Weber, W., Dincer, C., Urban, G.A., 2019a. Adv. Mater. 31, 1905311.

Bruch, R., Urban, G.A., Dincer, C., 2019b. Nat. Biomed. Eng. 3, 419-420.

Clavero C., 2014. Nat. Photon. 8, 95-103.

Chen, Q.M., Zhang, X.D., Li, S.Q., Tan, J.K., Xu, C.J., Huang, Y.M., 2020a. Chem. Eng. J. 395, 125130.

Ho, L.W.C., Liu, Y., Han, R.F., Bai, Q.Q., Choi, C.H.J., 2019. Acc. Chem. Res. 52, 1519-1530.

Hwang, M.T., Heiranian, M., Kim, Y., You, S., Leem, J., Taqieddin, A., Faramarzi, V., Jing, Y., Park, I., van der Zande, A.M., Nam, S., Aluru, N.R., Bashir, R., 2020. Nat. Commun. 11, 1543.

Kaisti, M., 2017. Biosens. Bioelectron. 98, 437-448.

Li, F., Pei, H., Wang, L.H., Lu, J.X., Gao, J.M., Jiang, B.W., Zhao, X.C., Fan, C.H., 2013. Adv. Funct. Mater. 23, 4140-4148.

Li, M.J. Xiong, C., Zheng, Y.N., Liang, W.B., Yuan, R., Chai, Y.Q., 2018. Anal. Chem. 90, 8211–8216.

Loo, A.H., Sofer, Z., Bouša, D., Ulbrich, P., Bonanni, A., Pumera, M., 2016. ACS Appl. Mater. Interfaces 8, 1951-1957.

Mal, A., Mishra, R.K., Praveen, V.K., Khayum, M.A., Banerjee, R., Ajayaghosh, A., 2018. Angew. Chem. Int. Ed. 57, 8443-8447.

Ouyang, X.Y., Liu, J.H., Li, J.S., Yang, R.H., 2012. Chem. Commun. 48, 88-90.

Parvin, N., Jin, Q., Wei, Y.Z., Yu, R.B., Zheng, B., Huang, L., Zhang, Y., Wang, L.H., Zhang, H., Gao, M.Y., Zhao, H.J., Hu, W.P., Li, Y.L., Wang, D., 2017. Adv. Mater. 29, 1606755.

Peng, Y.W., Huang, Y., Zhu, Y.H., Chen, B. Wang, L.Y., Lai, Z.C., Zhang, Z.C., Zhao, M.T., Tan, C.L., Yang, N.L., Shao, F.W., Han, Y., Zhang, H., 2017. J. Am. Chem. Soc. 139,

8698-8704.

Sun, H.J., Ren, J.S., Qu, X.G. 2016. Acc. Chem. Res. 49, 461-470.

Tang, Q., Zhang, Q.E., Jiang, Y., Li, J.S., Zheng, J., Li, Y.H., Yang, R.H., Tan, W.H., 2014. ACS Appl. Mater. Interfaces 6, 13470-13477.

Tavallaie, R., McCarroll, J., Grand, M.L., Ariotti, N., Schuhmann, W., Bakker, E., Tilley, R.D., Hibbert, D.B., Kavallaris, M., Gooding, J.J., 2018. Nat. Biotechnol. 13, 1066-1071.

Wang, C.X., Yu, P., Guo, S.Y., Mao, L.Q., Liu, H.B., Li, Y.L., 2016. Chem. Commun. 52, 5629-5632.

Wang, H., Ma, K., Xu, B., Tian, W.J., 2016. Small 12, 6613-6622.

Wang, H.H., Li, M.J., Wang, H. J. Chai, Y.Q., Yuan, R., 2019. ACS Appl. Mater. Interfaces 11, 23765-23772.

Wang, H.H., Li, M.J., Zheng, Y.N., Hu, T., Chai, Y. Q., Yuan, R., 2018. Biosens. Bioelectron. 120, 71-76.

Wang, M., Zhang, R., Li, J., 2020, Biosens. Bioelectron. 165, 112430.

Wen, S.P., Su, Y., Wu, R., Zhou, S.W., Min, Q.H., Fan, G.C., Jiang, L.P., Song, R.B. Zhu, J.J., 2018. Biosens. Bioelectron. 117, 260-266.

Willner, I., Baron R., Willner, B., 2007. Biosens. Bioelectron. 22, 1841-1852.

Yang, R.H., Jin, J.Y., Chen, Y., Shao, N., Kang, H.Z., Xiao, Z.Y., Tang, Z.W., Wu, Y.R., Zhu, Z., Tan, W.H., 2008. J. Am. Chem. Soc. 130, 8351-8358.

Zetsche, B., Gootenberg, J.S., Abudayyeh, O.O., Slaymaker, I.M., Makarova, K.S., Essletzbichler, P., Volz, S.E., Joung, J., van der Oost, J., Regev, A., Koonin, E.V., Zhang, F., 2015, Cell, 163, 759-771.

Zhang, B.T., Zhao, L.X., Lin, J.M., 2008. J. Environ. Sci. 20, 1006-1011.

Zhang, L.J., Luo, Z.B., Zeng, R.J., Zhou, Q., Tang, D.P., 2019. Biosens. Bioelectron. 134, 1-7.

Zhang, Y., Zheng, B., Zhu, C.F., Zhang, X., Tan, C.L., Li, H., Chen, B., Yang, J., Chen, J.Z., Huang, Y., Wang, L.H., Zhang, H., 2015. Adv. Mater. 27, 935-939.

Zhao, M.T., Wang, Y.X., Ma, Q., Huang, Y., Zhang, X., Ping, J.F., Zhang, Z.C., Lu, Q.P., Yu, Y.F., Xu, H. Zhao, Y.L., Zhang, H., 2015. Adv. Mater. 27, 7372-7378.

Zhao, W.W., Xu, J.J., Chen, H.Y., 2014. Chem. Rev. 114, 7421-7441.

Zhu, C.F., Zeng, Z.Y., Li, H., Li, F., Fan, C.H., Zhang, H., 2013. J. Am. Chem. Soc. 135, 5998-6001.

Zhu, Y.C., Li, Z., Liu, X.N., Fan, G.C., Han, D.M., Zhang, P.K., Zhao, W.W., Xu, J.J., Chen, H.Y., 2020. Biosens. Bioelectron. 148, 111836.

Graphical abstract

Fullerenol as a Photoelectrochemical Nanoprobe for Discrimination and Ultrasensitive Detection of Amplification-Free Single-Stranded DNA

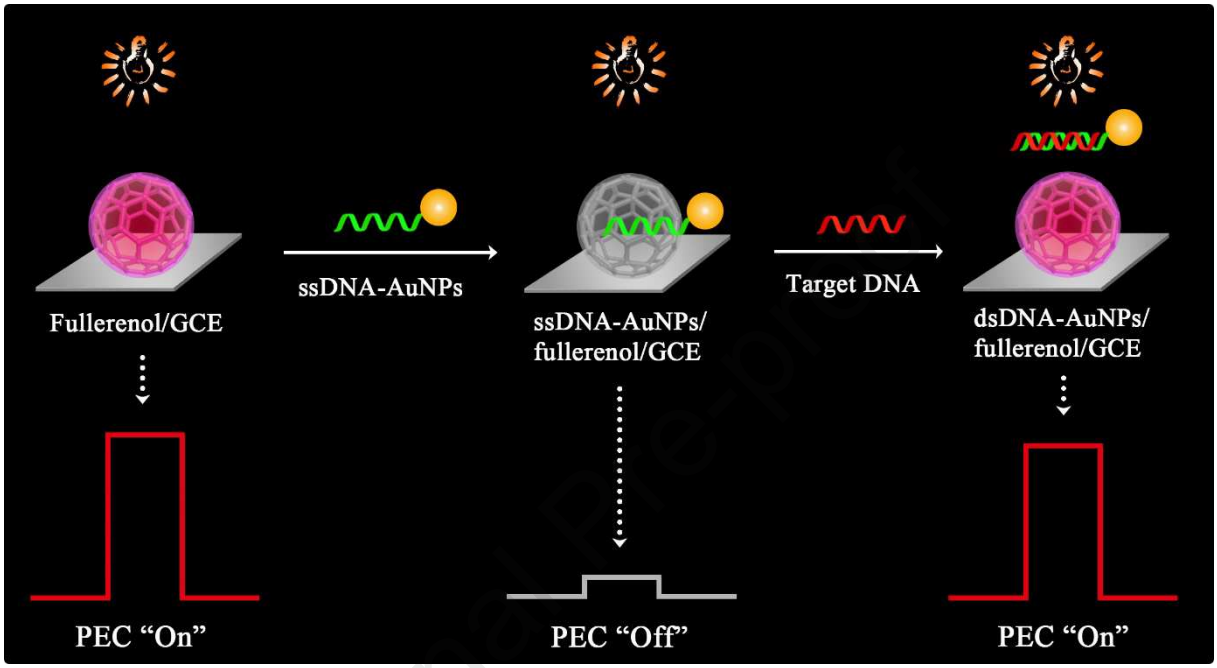

Highlights

Fullerenol as a Photoelectrochemical Nanoprobe for Discrimination and Ultrasensitive Detection of Amplification-Free Single-Stranded DNA

- Fullerenol as a PEC nanoprobe captured ssDNA but released dsDNA under the modulation of hydrogen bonding interactions.
- AuNPs owned signal quenching efficiency up to 85% against fullerenol *via* the visible light-induced electron transfer.
- The PEC biosensor achieved ultralow LOD down to sub-femtomolar level for target gene detection without prior amplification.
- This strategy represented a critical step toward the discrimination and ultrasensitive detection of nucleic acids.

Declaration of interests

☒ The authors declare that they have no known competing financial interests or personal relationships that could have appeared to influence the work reported in this paper.

☐The authors declare the following financial interests/personal relationships which may be considered as potential competing interests: